Molecular relaxation and microscopic structure of multilayers and superlattices of a photosensitive liquid-crystalline polymer

L. Cristofolini,[1] M. P. Fontana,[1] T. Berzina,[2] and O. Konovalov[3]
[1]*Dipartimento di Fisica and INFM, Università di Parma, Parco Area delle Scienze 7/A, I-43100 Parma, Italy*
[2]*INFM, UdR Parma, Parco Area delle Scienze 7/A, I-43100 Parma, Italy*
[3]*ESRF, Avenue des Martyrs, Grenoble, France*
(Received 16 May 2002; published 4 October 2002)

We report a detailed study of photoinduced changes in the microscopic structure of monolayers, multilayers, and superlattices of a photosensitive side chain liquid crystalline polymer, deposited by the Langmuir-Schaefer technique. We probe both out-of-plane and in-plane ordering and its changes due to optical pumping of the *trans-cis* photoisomerization transition of the azobenzene side chain in an azopolyacrylate. Microscopic structure was studied mainly by synchrotron radiation x-ray reflectometry and grazing incidence diffraction; we also used null-ellipsometry and atomic force microscopy. Our results provide a quantitative modeling of the structural changes and corresponding relaxation times taking place as a function of confinement, temperature and optical pumping, and in particular confirm previously reported ellipsometric results on such changes as a function of sample thickness. This allows a quantitative description of the effects of reduced dimensionality on the structural transitions in this glass-forming system.

DOI: 10.1103/PhysRevE.66.041801 PACS number(s): 68.47.Pe, 61.10.Kw, 61.30.Hn, 68.37.Ps

I. INTRODUCTION

The optical pumping of the *trans-cis* isomerization transition in polymeric systems containing the azobenzene moiety has received much attention in recent years, mainly because of applications to optical writing, potentially down to the nanoscale [1]. To this end, however, much fundamental study is still necessary, due to the complexity of the systems, which feature a rich phenomenology of relevance to phase transitions in liquid crystals, the glass transition, dewetting phenomena, the anomalous diffusional and vibrational dynamics in spatially heterogeneous systems. All of these issues can be studied in a specific class of these materials, namely side chain liquid crystalline polymers with an azobenzene moiety attached to the main polymeric chain via a flexible molecular spacer [2]. Here we shall mainly discuss the family of polyacrylates (similar results have also been obtained for polymethacrylates), in which the pumping of the photoisomerization transition yields several potentially useful optical effects with very high sensitivity [3], the vibrational and diffusional dynamics can be altered by the optical pump [4,6], the phenomenology of the glass transition has been extensively studied by calorimetric, dynamical analysis and ESR relaxation measurements [7]. Recently Langmuir-Blodgett (LB) technique [8] has been applied to obtain monolayer and multilayer of a specific system, namely, poly[[4-pentyloxy-3'-methyl-4'(6-acryloxyexyloxy)]azobenzene] (henceforth labeled PA4), which allowed the study of the effects of thickness on the structure and dynamics of the samples down to the nanoscale [9]. This was particularly relevant, not only to explore the potential for applications to nanowriting, but also to study a fundamental problem of long standing in the dynamics of disordered systems, namely the behavior of glasses in confined geometries or reduced dimensionality. Here the issue is the existence of so-called cooperatively rearranging zones [10], a model that provides a quantitative foundation to the classic Adam-Gibbs ansatz [11–13]. As the size of the system crosses the characteristic length of such zones, a disruption of the collective Adam-Gibbs behavior is expected. The experimental studies have been performed either in glassy systems confined in nanopores [14] or in ultrathin films [15–18]. In a recent paper [19] we have reported an ellipsometric study of the effects of restricted dimensionality on the glass transition of PA4 multilayers as a function of temperature. In this work the samples were perturbed by pumping the *trans-cis* photoisomerization transition, and the ensuing back-to-equilibrium relaxation was followed using real time null-ellipsometric probing of the thickness at several temperatures for samples of different thicknesses, ranging from one to sixty monolayers. We found a crossover in the sample behavior in the range of about eight monolayers: for smaller thicknesses, the data were interpreted in the framework of the so-called ''dead layer'' model [20,21] , in order to explain the observed divergence in the back-to-equilibrium relaxation times. The occurrence of important changes in structure and dynamics in ultrathin organic films below the thickness of about eight monolayers seems to be a fairly general occurrence, for which, however, we have not found any explanation in the literature. As the role of interfacial interaction is of paramount importance to the understanding of both the structure and the dynamics of thin polymeric layers, we also explored other structures of confinement of molecular layers of the photosensitive polymer; namely, we deposited superlattices where we obtained homogeneous confinement of the polymer by intercalation of fatty acid salts bilayers.

In this paper, we wish to address these points more extensively and seek quantitative confirmation of our previous results [19], and at the same time extend our study to include a quantitative experimental analysis of the effects of interactions with the substrate, and of the presence of the free surface (the ''extrinsic'' effects) on the observed phenomenology, in order to extract the intrinsic behavior as a function of

thickness. We have also studied photoinduced dewetting phenomena, not only to identify and separate their eventual effects on our observations, but also as an interesting pathway to produce by optical means nanoparticles of our polymeric glass in a reasonably controllable fashion.

The experimental techniques we used to obtain information on the microscopic structure of the deposited architectures are x-ray reflectometry, which yields the out-of-plane structure, i.e., in the direction perpendicular to the substrate, and x-ray grazing incidence diffraction, which yields the in-plane structure. We have also used null-ellipsometry and atomic force microscopy (AFM) to further characterize our samples, to provide complementary information on thickness and morphology, and to image the photoinduced or temperature induced dewetting in our films. Finally, we have performed preliminary null-ellipsometry static and kinetic experiments to study the photoinduced effects on the Langmuir monolayer at the air water interface and their temperature dependence.

We have prepared three different types of molecular architectures, namely:

(i) monolayers and multilayers of PA4 on silicon covered by its natural oxide or on silanized silicon;

(ii) the same but deposited on a highly hydrophobic substrate made up of a bilayer of Ba-behenate on silicon, with and without covering of the air interface by inert bilayer of Ba-behenate; and

(iii) multilayers of polymer of different thickness sandwiched between bilayers of the Ba-behenate molecular separator, to yield a superlattice structure, with periodic repetition of the Ba-behenate bilayers obtained by the Langmuir Blodgett (LB) deposition technique alternated by PA4 multilayers obtained by the Langmuir-Schaefer (LS) deposition technique.

The rationale for these choices was that in samples of the first type we study the simpler system, in which, however, we have no control of both interactions with the substrate and the effects of the free surface; in the second type, we control the interaction with the substrate more precisely, and we can separate the contribution arising from the presence or absence of a free polymeric surface. In the third type, we eliminate completely the free surface and control the interaction with the confining media. Moreover, the last structure is particularly suitable for the study by x-rays reflectometry, due to the large contrast in scattering length density between the layer containing the Ba^{2+} ions and the surrounding organic medium.

Finally, we have also studied photoinduced effects on the Langmuir monolayer at the air water interface. Clearly this is, as close as we can get to a two dimensional system, even though the real situation may not be quite as simple, since such monolayer is stabilized by the interactions with the water subphase.

II. EXPERIMENT

A. Sample preparation

The polymer PA4 was synthesized and characterized according to procedures already reported in the literature [22]. Its mean molecular weight was $M_w = 19\,000$, $M_n = 12\,000$ (weight and number averaged, respectively). The other compounds were purchased from Sigma-Tau and used without further purification. The deposition was performed using a modified [23] horizontal lifting (Langmuir-Schaefer, LS) technique, which allowed the rapid and uniform deposition of many monolayers onto a silicon substrate. This is essential to obtain a film, as free as possible from defects. The substrate used was either covered with native oxide, or was treated with dimethylchlorosilane to make it hydrophobic. We first studied the pressure-area ($\Pi - A$) isotherm of the Langmuir monolayer on a KSV5000 Langmuir system, then we chose the optimal surface pressure ($\Pi = 15$ mN/m at room temperature) for the deposition of the Langmuir-Schaefer multilayers. The deposited films were routinely characterized by optical microscopy, by Fourier Transform Infrared and optical absorption spectroscopy. A more detailed description of experimental techniques can be found elsewhere [24]. Using the same techniques the superlattices were prepared. In this case the deposition sequence was: first a bilayer of Barium behenate, then n monolayers of PA4 ($n = 1,4,6,8,10$), then another bilayer of Ba-behenate. This unit was repeated for several times to create the superlattice structure. We also studied the basic unit, with or without the external Barium behenate bilayer.

B. Structural measurements

X-ray reflectivity (XRR) experiments were performed on the beamline ID10b (Troika-2) at the ESRF synchrotron facility operating at the wavelength $\lambda = 1.385$ Å. During the measurement rocking curves were frequently taken to test the level of diffuse background and identify the true specular reflectivity. In the following, data are truncated in Q_z in order to show the true specular reflectivity only.

The sample was placed in a helium-flushed chamber with the temperature controlled by means of a Peltier cell [T stability within ± 0.1 K). For the *cis-trans* isomerization we used a filtered high-pressure Hg lamp placed on top of the sample, at a distance of 10 cm.

Grazing incidence diffraction (GID) patterns were collected with the incident beam impinging at $\theta = 0.18°$ from the sample surface, i.e., below the critical angle for total reflection of the substrate; this minimizes a possible contribution to the GID signal from the substrate, which could be a problem at the smallest thickness of the deposited polymeric layers. The signal was then integrated in the vertical direction by means of a position sensitive detector (PSD) over the range Q_z from 0 to about 0.3 $Å^{-1}$. In selected cases a second and a third scan were performed with the PSD detector at higher angle to extend the explored Q_z range.

Here we must note that care had to be taken that the incoming flux of x rays did not damage or otherwise modify our fragile and metastable samples. For this we took repeated runs on the same sample, and noted the eventual changes in the reflectivity pattern. We found substantial effects on the high-Q side, clearly due to the geometry induced higher power density there. Thus we truncated our patterns at the wave vector values below which the radiation effect was

negligible. For this we also had to reduce the overall counting time, compatibly with an acceptable signal-to-noise ratio.

Sample thickness and its variations were also determined by null ellipsometry. Our techniques and procedures have been described in previous publications [19,24]. Here we remark that the overall uncertainty associated with the x-ray reflectivity and ellipsometric measurements is larger than the pure instrumental uncertainty, which is due to mechanical hysteresis, positioning reproducibility and stability and so on, which, however, in our case is better than 0.1 Å. Neither uncertainty stems from individual sample lateral inhomogeneity, but is mainly due to the reduced reproducibility of the behavior from sample to sample of such complex system of liquid crystalline photosensitive polymer. To improve reproducibility we strictly adhered to a protocol of sample preparation, storage in dark at room temperature for not less than 12 h and not more than 5 days and careful thermal annealing prior to any characterization.

The ellipsometric measurements on the Langmuir monolayer were performed by placing a small trough directly in the path of the laser beam of the ellipsometer. The trough was mounted on a platform whose vertical position could be finely regulated with a micrometric screw. The optical pump was a mercury lamp situated ≈ 10 cm above the liquid surface. The temperature dependence data were difficult to obtain, since as the temperature was increased; liquid evaporation rate increased: at the sensitivity level of our measurements, this made the detection of the real ellipsometric signal impossible. Thus we had to humidify the air, surrounding the apparatus to minimize the evaporation and hence stabilize the liquid level on the trough, for enough time to be able to record the signal at a given temperature in the two conditions of darkness and illumination. This proved to be possible only up to about 40 °C with the available setup.

Finally, surface morphology and sample thickness on the nanoscale have been probed by AFM imaging in the noncontact mode. For this we used an Autoprobe CP Research instrument from Thermomicroscopes equipped with a large area (100 μm) scanner with optical feedback for the independent control of the lateral movements of the piezo scanner. We used Ultrasharp noncontact silicon cantilevers (from Silicon-MDT Ltd.) with nominal curvature about 10 nm, and typical resonance frequency 150 KHz. Unless differently specified, all the measurements were performed at room temperature and strictly in the dark; particular attention was paid to the latter point: the light source for the optical observation of sample and AFM tip was used at the minimum, and it was red-filtered in order to eliminate all the green-blue components that are known [5] to affect the azobenzene moiety.

Finally, a useful quantity to characterize the surface roughness and its evolution under the effect of different factors is the root mean square roughness σ_{RMS}, calculated over all the points of the measured surface.

III. RESULTS AND DISCUSSION

A. Simple PA4 multilayers

We shall begin by presenting our results on the simple PA4 multilayers. In Fig. 1 we show the x-ray reflectivity data taken on the pristine sample at room temperature as a function of the number of deposited monolayers (i.e., sample thickness).

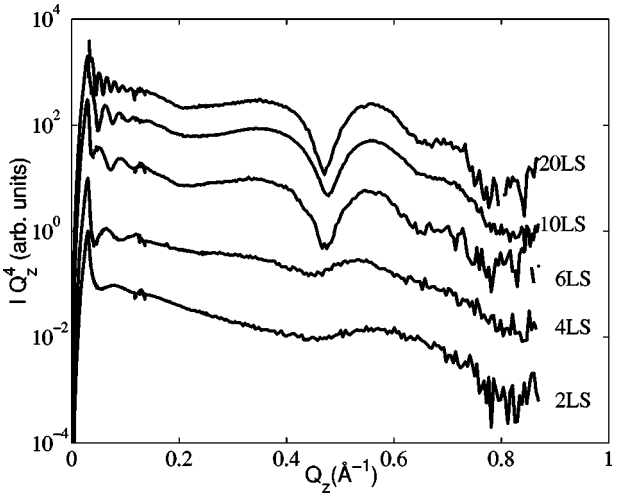

FIG. 1. Reflected intensity measured at room temperature and scaled by Q_z^4 from multilayers of different thickness (2, 4, 6, 10, and 20 molecular layers) of PA4 deposited on natural silicon.

The most noticeable feature is the appearance of a broad dip at about 0.48 Å^{-1}, as the thickness increases above six layers. Note that the width of the dip appears to decrease as the number of layers is increased. We also note that the Kiessig fringes, although clearly visible, are strongly damped, especially for the thinner samples.

We calculate the intensity reflected by our complex layered structure by applying either the matrix approach or the recursive Parrat algorithm [25]. Layer roughness is accounted for by the Nevot-Croce approximation [26], appropriate for roughness with small (<1 μm) lateral coherence, the reflectivity of the interface between media j and $j+1$ is then scaled by the Nevot-Croce factor F;

$$F=\exp(ik_{z,j}k_{z,j+1}\sigma_j^2), \tag{1}$$

where $k_{z,j}$ is the z component of the wave vector in medium j and σ_j is the roughness of the corresponding interface j. Such an approach requires a preliminary guess about the elements of the model. This can be done by inverse Fourier Transformation (FT) of the reflected intensity $R(Q)$ at the exchanged wave vector Q, which, in the kinematic (Born) approximation, is simply related to the modulus of the FT of the gradient along the z direction of the refractive index n:

$$R(Q)=R_F\left|\int \frac{\partial n(z)}{\partial z}\exp(iQ_z)dz\right|^2. \tag{2}$$

Therefore, after careful normalization one can hope to be able to extract, in a model-free fashion, the distances between the various interfaces.

After normalization to the reflectivity of the bare substrate, we obtained a structured (layered) variation in the refractive index, which is associated with the ''typical'' distances of 23, 37, and 50 Å. We then refined this model either by using the PARRAT32 software [27] or double checking our

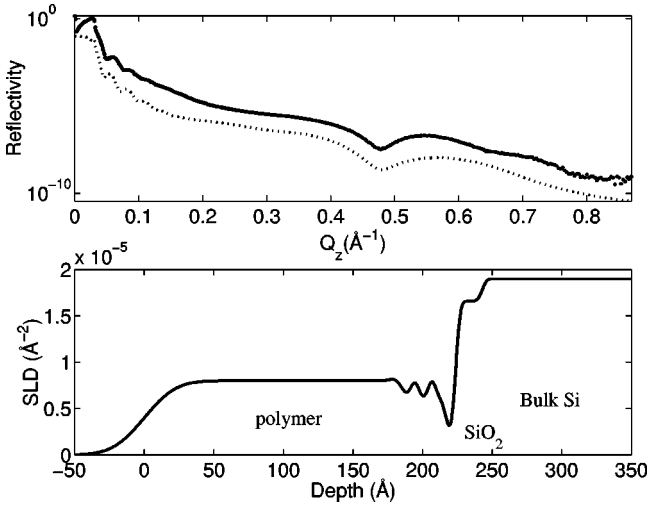

FIG. 2. Top panel: fit (dotted line, down-shifted by a factor of 10) of the measured reflectivity on a film made of ten monolayers of PA4 at T=RT. Bottom panel: the model of scattering length density (SLD=$r_0\rho_e$, $Å^{-2}$, see text for details) employed to fit the experimental data.

results with software developed by one of us [28]. The resulting theoretical intensity and structural model are shown in Fig. 2, top and bottom panels, respectively. The substrate is modeled as bulk Si covered by 19 Å thick native oxide, the scattering length density (SLD=$r_0\rho_e$) values of which are known from the literature. The polymeric film is made up of a first series of pseudoperiodic, layered units of thickness 13.5 Å, with zones of alternating high and low SLDs. In particular the interface between the silicon oxide and the polymer shows a minimum SLD density, followed by a region of higher density. This structure is repeated three or four times with decreasing contrast between high-SLD and low-SLD regions. At larger distance from the substrate the polymeric film is unstructured and has an average SLD $\sim 0.910^{-5}$ $Å^{-2}$, a reasonable value if compared to that of pure PMMA (SLD=1.0810^{-5} $Å^{-2}$) [29]. The film-air interface has roughness $\sigma \sim 20$ Å.

Similar results were also found for films deposited onto silanized hydrophobic substrates. We note in passing that other possible fitting models, such as crystalline regions embedded in an amorphous matrix, did not yield fits of the same quality, and have been discarded also on the basis of all the other knowledge that we have on this polymeric system.

Thus the structural model that seems to fit the data better consists of three components: the oxide covered silicon substrate, the homogeneous polymer film, and an intermediate, crystallinelike zone composed of up to about four polymeric layers. This is most remarkable, and provides direct confirmation of the so-called dead layer hypothesis that we used in our previous work [19] to interpret the ellipsometric data.

These results were independently checked by null-ellipsometric measurements on the same homogeneous multilayers. The results are summarized in Table I in which the thickness of the polymeric layer is varied from only 4 to 100 monolayers. The homogeneous character of the deposition over the whole thickness range explored is evident from the proportionality between the thickness t and the number of deposited layers n.

TABLE I. Thickness and photoinduced expansion, as measured by null-ellipsometry, below the glass transition temperature T_g of homogeneous layers of PA4 consisting of n monolayers.

n	Thickness t (Å)	δt (Å)	$\delta t/t$
4	70.6	4.5	0.064
10	176.0	17.1	0.097
20	333.8	33.0	0.099
60	1441.8	147.7	0.102
100	1930.0	170.0	0.088

B. Isothermal photoinduced structural effects

We come now to the presentation of the photoinduced structural effects. In Fig. 3 we show the reflectivity pattern of the ten layer sample at room temperature before and under illumination with UV light. Clearly the microscopic structural changes induced by the *trans-cis* photoisomerization are quite strong.

There are two spectacular effects: one is the total disappearance of the dip at 0.48 $Å^{-1}$ and the other is the much larger Q_z range of the Kiessig oscillations. From the damping of the oscillations we have calculated a mean square roughness of about 10 Å. Thus the UV illumination has a pronounced smoothing effect, reducing the mean surface roughness by a factor of two. This fluidification effect of the *trans-cis* isomerization pump had already been hypothesized on the basis of optical data [30]; here it is beautifully confirmed. This by the way excludes that our observations might be due to dewetting, which would cause an increase in the

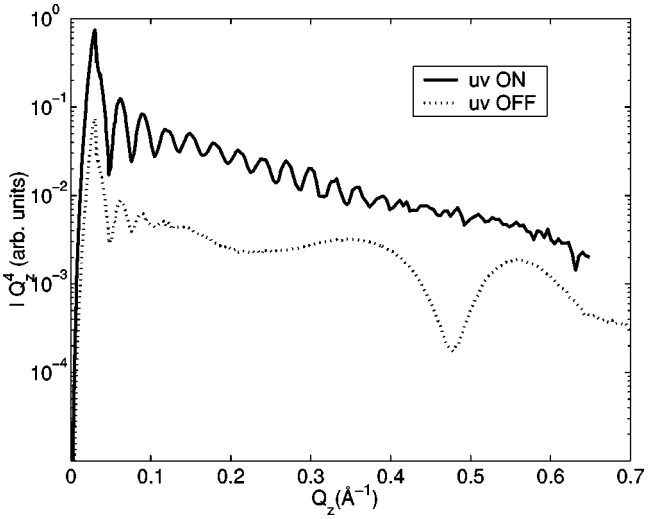

FIG. 3. Photoinduced changes in the x-rays' reflected intensity of a ten layer sample of PA4 measured at T=RT. Dotted line, film before UV irradiation. Continuous line, film during UV irradiation. Note upon UV illumination the reduction of roughness, indicated by the extension of the Kiessig fringes, and the disappearance of the feature around $Q_z=0.48$ $Å^{-1}$.

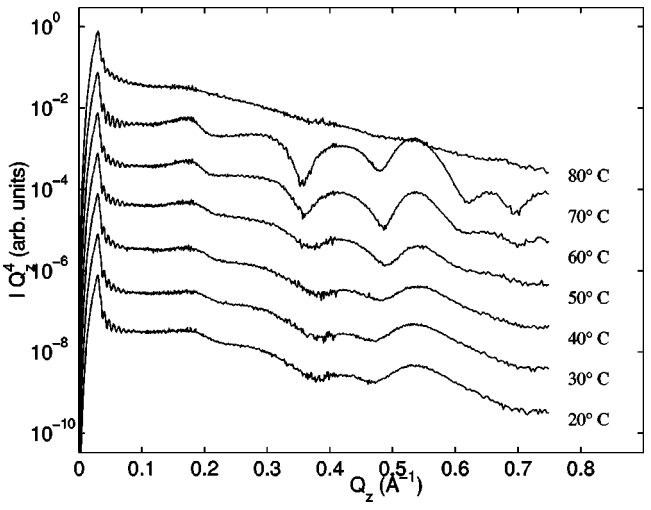

FIG. 4. Reflectivity curves of a film of 40 monolayers of PA4 as a function of the temperature. The onset of the nematic phase and its melting are responsible for the appearance of the features at $Q_z > 0.3$ Å^{-1} and for their evolution.

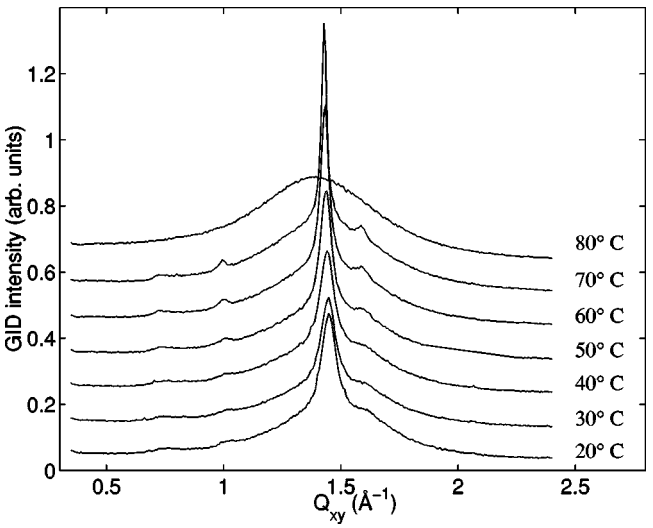

FIG. 5. GID pattern from a sample made of six monolayers of PA4 at selected temperatures. It is evident from the data that the nearest neighbor correlation peak sharpens upon heating until the final melting of the multilayer is reached at about 80 °C.

apparent roughness. This point will be discussed in greater detail with the AFM data.

Moreover by x-ray reflectivity we could confirm the ellipsometric result [19] that below the glass transition temperature the photoexpansion reaches an equilibrium maximum value of 1–2 Å per monolayer, i.e., roughly 5–10 % of the overall film thickness, independent of film thickness. This agreement is further extended by the present ellipsometric results, summarized in Table I, where the third column reports the photoinduced expansion, and the fourth column reports the same quantity normalized to the total film thickness. We note, however, a small deviation from the average behavior of the thinner film (four monolayers); this is outside the experimental uncertainty, which is less than 1 Å, and could be related to the quasi periodic layering of the monolayers deposited closer to the fatty acid spacers. However, photoinduced expansivity varies from sample to sample, also for the thicker samples, so that only a broad range of variation (5–10 % of the overall film thickness) can be indicated. The important qualitative result, however, is that photoexpansivity is an extensive quantity, i.e., it roughly scales with the number of deposited layers, and is not a surface related property, which would be roughly independent of film thickness, at least above some threshold.

C. Temperature dependence

Let us recall that in the bulk phase [7], our polymer melts into a nematic phase at 78 °C and has a nematic to isotropic clearing point at 96 °C. We have tried to verify the microscopic structural changes accompanying these transitions In Fig. 4 we show the reflectivity scaled by the fourth power of the exchanged momentum Q_z^4, for a multilayer (40 layers) of PA4 as a function of temperature; data are taken upon heating. The development of the structures at $Q_z > 0.3$ Å^{-1} in the reflectivity curves measured above 40–50 °C is related to the onset of the glass to nematic phase transition, occurring at 78 °C. The melting of the glassy phase results in the flat, featureless reflectivity curves measured at $T = 80$ °C, which implies a disruption of the periodicity along the z direction, typical of the nematic phase. We note in passing that the roughness of the top and bottom interfaces is the same for all the temperatures, as can be evaluated by the damping cutoff of the Kiessig fringes. In Fig. 5 we report the grazing incidence diffraction (GID) signal obtained from a multilayer ($n = 6$ layers) of PA4 deposited onto hydrophobic Si, at different temperatures. While at $T = 20$ °C the GID signal consists mainly of one broad peak of almost Lorentzian shape centered at $Q_{xy} = 1.44$ and a shoulder at $Q_{xy} = 1.60$ Å^{-1}, as the temperature is increased the GID peaks become narrower and better defined, and further, much weaker shoulders appear at $Q_{xy} = 1.0$ Å^{-1}, and 1.65 Å^{-1}.

The change of the GID signal is consistent with that of the reflectivity curve, the sample becomes better structured as the temperature is increased, before melting, both in the normal to surface and in the in-plane direction. Moreover, we can infer that a minority part of our sample undergoes crystallization upon heating, as we observe a transition from hexagonal packing to a generic monoclinic cell, while all the rest remains in a liquidlike state giving rise to the broad background observed under the sharp peak in the GID pattern. This latter point is under current investigation. Finally at $T = 80$ °C the sample becomes nematic, with no long-range positional order, and a broad unstructured peak appears, characteristic of this phase.

D. Superlattices: x-ray reflectivity and ellipsometry

To understand the role of geometric and interfacial interaction in determining the observed anomalies in the structure of the first layers of polymer, we studied superlattice structures in which the photosensitive polymer was confined between inert fatty acid bilayers.

By null ellipsometry we have measured the overall superlattice thickness, as reported in third column of Table II.

TABLE II. Thickness t, photoinduced expansion δt, and normalized photoinduced expansion $\delta t/t$ at $T=19\,^{\circ}\mathrm{C}$ of superlattices [2 LB BaBeh: l LS PA4]$_n$.

n	l	Total t (Å)	δt (Å)	$\delta t/t$
1	10	166	19	0.114
2	10	464	20	0.043
3	10	707	19	0.026
4	10	1005	21	0.021
10	10	2490	27	0.010

Then we measured the photoinduced structural changes, following photoperturbation by UV light. In the fourth column of Table II we report the photoinduced thickness increase δt, whereas the last column reports the same quantity normalized to the overall thickness.

As it is easily verified, δt is independent of the number of repeated units in the superlattice. Moreover, if one assumes the standard value for the photoexpansion (1–2 Å per monolayer of polymer) as measured by both XRR and ellipsometry on homomultilayers (see, discussion of the data of Table I), then the measured photoexpansion is compatible with expansion of the topmost polymeric layer only.

We also measured the x-ray reflectivity of such superlattices, as shown in Fig. 6, and found no significant variation of the reflected intensity upon UV illumination. In particular both Bragg peak positions and Kiessig fringes spacing are practically unaffected by the UV illumination, whose main effect seems to be that of smearing out the high-Q side of the curve, perhaps due to a combination of radiation damage and surface alterations. As a matter of fact, x-ray reflectivity mainly probes the periodic repetition of the layers containing the Ba^{2+} ions in the bulk of the film, which is not affected by the expansion of the uppermost repeated unit. Therefore, the XRR observation is a confirmation that, in superlattices, photoexpansion only takes place in the uppermost repeated unit, whereas the other repeated units seem to retain their own structure and periodicity.

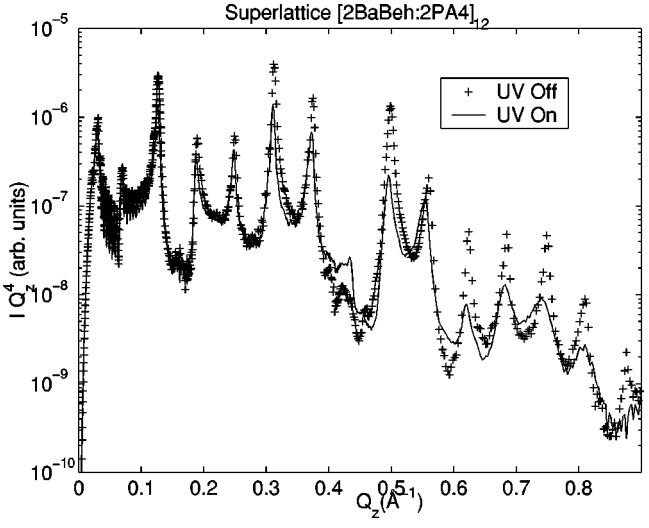

FIG. 6. Reflected intensity measured at room temperature and scaled by Q_z^4 from a superlattice structure [2 LB BaBeh: 2 LS PA4]$_{12}$. Crosses, reflectivity measured on the pristine sample; line, reflectivity under UV illumination.

TABLE III. Same as above in a single repeated unit, both as *open* and as *closed* structures [2 LB BaBeh: l LS PA4] and [2 LB BaBeh: l LS PA4 2LB BaBeh], respectively.

l	Open/closed	Total t (Å)	t_{PA4} (Å)	δt (Å)	$\delta t/t_{PA4}$
2	open	102.4	43.0	3.1	0.072
2	closed	155.3	36.5	1.1	0.030
4	open	125.1	65.7	4.2	0.064
4	closed	188.0	69.2	3.73	0.054
6	open	155.6	96.2	6.84	0.071
6	closed	218.9	100.1	6.59	0.066
10	open	246.6	187.2	16.5	0.088
10	closed	309.1	190.3	14.3	0.075
20	open	417.2	357.8	29.3	0.082
20	closed	467.0	348.2	26.7	0.077

The question then arises whether the photoinduced expansion is hindered or not when the interface between the photosensitive polymer and air is not a free surface, but is blocked by an inert layer, such as Ba-behenate. In Table III we report the thickness and the photoinduced expansion of a single repeated unit, both as *open* and as *closed* structure, realized by [2 LB BaBeh: l LS PA4] and [2 LB BaBeh: l LS PA4 2LB BaBeh], respectively. We report both the total thickness t, as obtained by the ellipsometric measurement, and the polymeric thickness t_{PA4}, obtained after subtraction of the fatty acid layers, 59.4 Å per bilayer of Barium behenate (BaBeh), value obtained by measuring pure BaBeh multilayers by both null-ellipsometry and x-rays reflectivity. The next column δt is the photoinduced thickness increase, whereas in the last column we report the same quantity normalized to the polymeric thickness t_{PA4}. At first sight it is clear that photoexpansion is observed both in the presence and in the absence of covering inert topmost layer. This implies that photoexpansion is a volume effect, which takes place over the whole film thickness [35]. A detailed analysis, however, reveals that the photoinduced expansion of the *open* structures is about 10% systematically higher than that of the *closed* structures. Therefore, we think that the high-mobility liquidlike layers at the air interface exhibit larger rearrangements upon photoperturbation. This is a confirmation of the complexity of the behavior of such photosensitive liquid crystalline polymeric system, in which volume effects and surface effects are intimately entangled and takes place on the same scale.

E. Superlattices: Grazing incidence diffraction

In Fig. 7 we show the grazing incidence diffracted intensity by a superlattice structure of ten monolayers of PA4 intercalated between bilayers of Ba-Behenate at the temperature $T=11\,^{\circ}\mathrm{C}$, data are shown as a function of both the in-plane (Q_{xy}) and the out-of-plane (Q_z) exchanged mo-

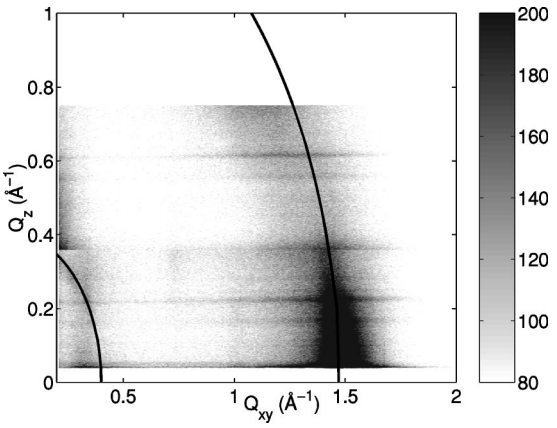

FIG. 7. In-plane (Q_{xy}) and the out-of-plane (Q_z) dependence of the intensity diffracted by a superlattice structure of ten monolayers of PA4 intercalated between bilayers of Ba-Behenate at $T=11\,^{\circ}\mathrm{C}$. The two line arcs represent Debye rings, as discussed in the text.

menta. In order to extend the Q_z range, we combined two data sets acquired with two horizontal scans performed at different zenithal angles.

The most prominent feature is the peak at $Q_{xy}=1.47$ Å^{-1} at $Q_z=0$ Å^{-1} (darker area on the lower part of the figure), which corresponds to a nearest neighbor distance of 4.3 Å. This peak is, relatively broad (FWHM $=0.17$ Å^{-1} which would correspond to a coherence length of up to ten lattice units). We have already commented upon the temperature dependence of the width, in the previous Sec. III C. Here we note that the dependence of the scattered intensity from the out-of-plane and in-plane components of the exchanged momentum resembles more a Debye ring, as indicated by the circle overimposed to the data, than a Bragg rod, which would appear as a vertical line in the same figure. We take this as an indication of, relatively large tilting between the different layers, or more generally, of nonideal order along the vertical direction.

The patterns reported in the figure are only slightly modified by the optical pumping; it appears that when the polymer multilayers are sandwiched in the the behenate ''crystal,'' they are much less sensitive in their structure and morphology to the effects of the photoisomerization cycle. This is consistent with the findings of the previous section, that photoperturbation in superlattices acts only on the topmost period, whereas GID probes the full set of layers. Therefore, any possible photoinduced modification of the topmost layer would result in little or no change on the overall GID pattern.

F. Atomic force imaging

Pristine films deposited at high surface pressure ($\Pi=15$ mN/m) show a morphology mainly due to incomplete topmost coverage. A typical topography is shown in Fig. 8; the vertical contrast scale is 8 nm. The corresponding root mean square roughness is $\sigma_{RMS}=1.66$ nm, a value which nicely corresponds to the RMS roughness as estimated independently from the damping of the Kiessig fringes in the x-ray reflectivity experiment. The terraces (lighter areas) correspond to regions covered by the uppermost molecular layer, whereas the valleys (darker areas) are regions not covered by the uppermost layer. The valley-to-terraces height difference (2.7 nm) corresponds to the thickness of the uppermost layer. The deposition of a very rigid (and brittle) Langmuir layer, as indeed is the film of PA4 at high pressure, reasonably occurs via ''rigid patches'' that deposit with no deformation but rather with many cracks, as observed in the AFM image.

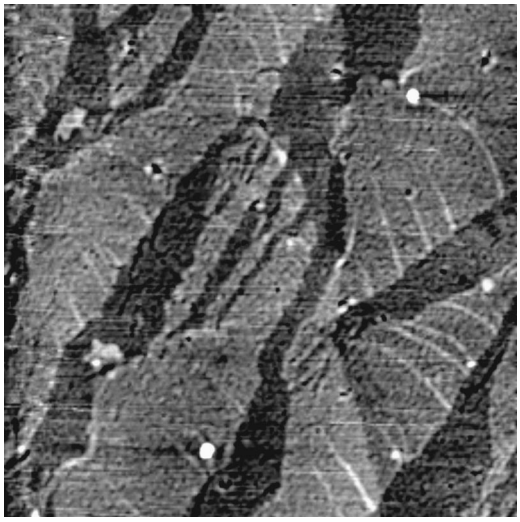

FIG. 8. AFM image of a film as deposited at high surface pressure ($\Pi=15$ mN/m). The horizontal scale is 6×6 μm^2, the vertical contrast scale is 8 nm. The terraces (lighter areas) correspond to regions covered by the uppermost molecular layer, whereas the valleys (darker areas) are regions not covered by the uppermost layer. The valley-to-terraces distance (2.7 nm) corresponds to the thickness of the uppermost layer.

In order to check this point, we also measured the morphology of films deposited at much lower surface pressure ($\Pi=1$ mN/m), where the film is not so rigid. A nice ex-

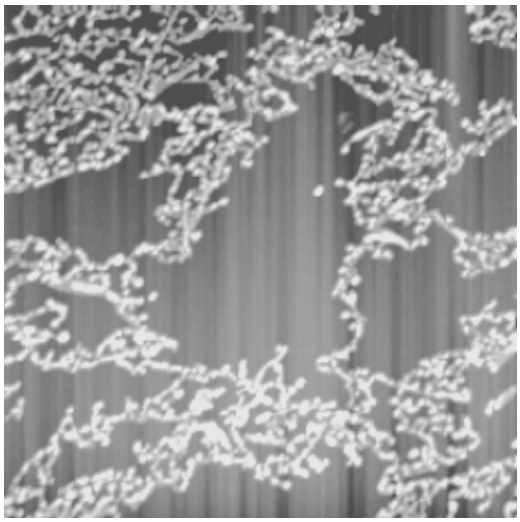

FIG. 9. 6×6 μm^2 AFM image of a film deposited at low pressure ($\Pi=1$ mN/m).

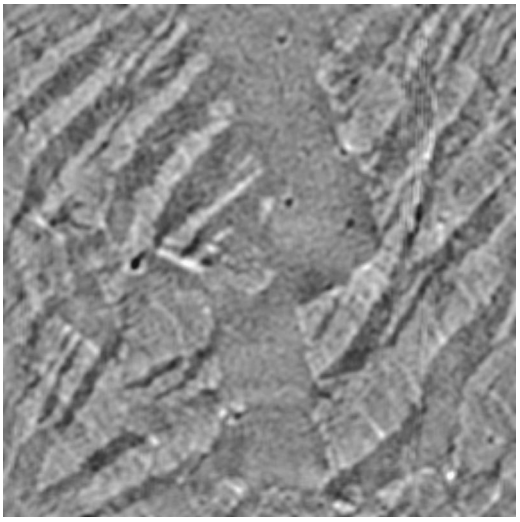

FIG. 10. AFM image of a film of PA4 after 15 min exposure to UV radiation. Lateral scale is 6×6 μm^2, the vertical contrast corresponds to 8 nm.

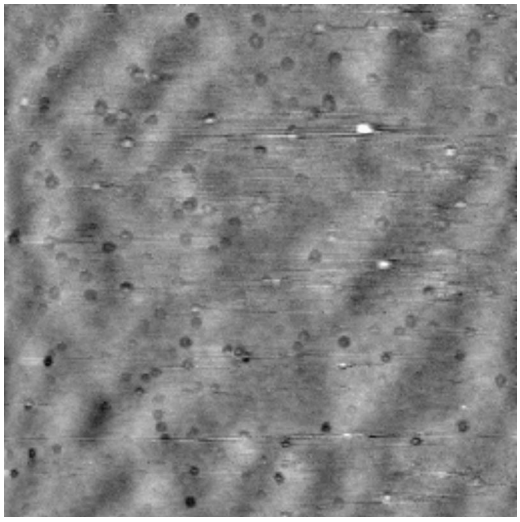

FIG. 11. AFM image of the same film of PA4 after 1 h exposure to UV radiation. Lateral scale is 6×6 μm^2, the vertical contrast corresponds to 8 nm.

ample is shown in Fig. 9: we do observe aggregates of bubbles, the size of each bubble being comparable with the estimated size of a single polymeric chain. The bubbles indeed form threadlike aggregates, with typical lateral size about 100 nm and length extending to several microns.

Returning now to the films deposited at higher surface pressure, exposure to UV light from a filtered Hg lamp first reduces surface roughness, reducing the terraces, as shown in Fig. 10, which has lateral size 6×6 μm^2, and vertical contrast of 8 nm. The root mean square roughness is $\sigma_{RMS}=0.9$ nm in this image. The observed reduction of a factor of 2 for the surface roughness is in good agreement with the independent results from x-ray reflectivity. We believe that the physical origin of the surface smoothing relies on the fluidification effect that the *cis* isomer has on the polymer, as independently confirmed by inelastic neutron scattering [6], and by measurement of photoinduced birefringence [30]. Such effect is very likely connected with the more isotropic shape of the *cis* conformer of the azobenzene moiety, and with the poisoning of the nematic phase when the concentration of *cis* conformers becomes important.

The same fluidification effect is responsible for the dewetting that takes place when UV exposure is extended to longer time scales, as shown in Fig. 11, in which the roughness would be completely smoothed, but round holes start to develop. The number density and the size of the holes grows as the UV exposure is extended, and so does the size distribution, until a granular morphology is reached, wherein each grain is a polymeric bundle of approximate mean size of 2–3 nm. Thus by excitation of the photoisomerization transition we can use the dewetting phenomenon to create glassy nanoparticles, with the potential for a detailed control of size distribution and morphology by appropriate variation of parameters such as temperature, light power density and wavelength, time and sample thickness. Work on this aspect of the problem is in progress.

IV. LANGMUIR MONOLAYERS AT THE AIR WATER INTERFACE

The confined geometry of the monolayer at the air water interface is perhaps the closest approximation to a two dimensional system, especially when the monolayer is compressed to its pseudosolid phase; here in fact the intermolecular and intramolecular interactions involving only the polymer molecules should become more important in determining the structure and dynamics, and to a first approximation we can disregard the interactions with the aqueous subphase. Thus in this configuration we may expect to minimize the problems connected with the substrate and free surface interactions and effects. From the point of view of the glass transition of course it remains to be seen to what extent the compressed monolayer can be described as a glassy solid. In what follows we shall present some preliminary data that indicate that this might be the case, and that glass transition concepts can be used to interpret the data.

In Fig. 12 we show a typical isotherm of the PA4 monolayer, in the dark and under UV illumination. The abscissa is area per monomeric unit. The strong alteration induced by UV light confirms the fluidification effect induced by the photoisomerization of the azobenzene side chains.

A scaling analysis can be applied to these isotherms [31,32]. In the semidilute regime the surface pressure can be expressed as [32,33]

$$\Pi=\Gamma^{y}, \tag{3}$$

where Γ is the concentration of molecules per unit of surface area, and y is a scaling exponent related to the Flory exponent ν, relating the chain radius of gyration R_g to the number of monomers N: $R_g\approx N^{\nu}$. The Flory exponent ν is connected to y by $y=2\nu/(2\nu-1)$ in two dimension (2D). In particular in 2D one expects $\nu=1$ for the extended chain, and to decrease to $\nu=4/7$ for θ solvent, and to $\nu=1/2$ for the

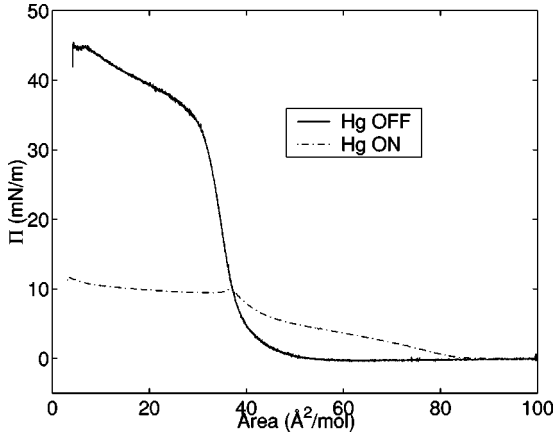

FIG. 12. Compression isotherms ($T=19\,^{\circ}\mathrm{C}$) of PA4 in dark (continuous line) and under UV illumination (dot-dashed line). Abscissa, area per monomeric unit

poor solvent condition, respectively. Correspondingly y takes the values of 2, of 8, and of infinity. This was first verified for a polymer monolayer by Vilanove [34] and has since been applied to a wide range of polymer monolayers [31].

In Fig. 13 we show the isotherm in scaling form for the monolayer in the dark and after illumination by filtered UV light. The scaling picture emphasizes dramatically the effects of the *trans-cis* photoisomerization on molecular interactions within the monolayer. In particular we note that the scaling exponent changes from about ten to two upon optical pumping; this implies a change in the interaction with the aqueous subphase, from a situation almost of theta solvent to that of good solvent, respectively. Such behavior can be understood on the basis of the difference in the properties of the azobenzene side chain in the two conformations: the *cis* isomer has a strong dipole moment (3–5 Debye), in contrast to the 0.5 Debye of the *trans* isomer. Thus the monolayer with a strong

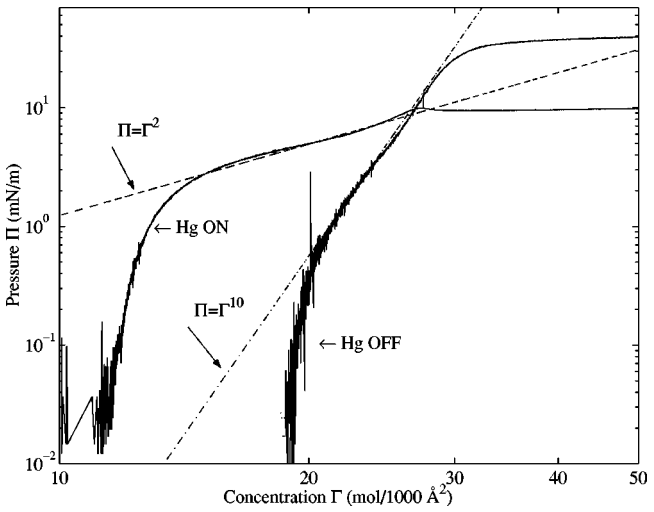

FIG. 13. Scaling law for the compression isotherm of PA4 measured at $T=21\,^{\circ}\mathrm{C}$ with and without UV photoperturbation (see text for details). Dashed lines correspond to the scaling laws $\Pi=\Gamma^{y}$ with $y=2$ and 10, respectively, typical of a very favorable interaction with the subphase and of almost θ solvent condition.

population of *cis* isomers can be expected to have stronger long-range interactions, hence the surface pressure will start rising at smaller surface densities, as demonstrated clearly in the isotherms reported in Fig. 12. Clearly the monolayer with strong dipole moment moieties will also be expected to show good solvent behavior, in agreement with the observed change in the scaling exponent upon optical pumping. We must note, however, that such a scaling law analysis is valid only in a region of the pressure-concentration plane; its validity is limited at high pressure, high concentration, by the onset of side chain interactions, and it also fails in the very low surface pressure region, possibly due to errors unavoidably associated with the measurement of very low surface pressure.

We have then followed the back relaxation process after *trans-cis* conversion in the monolayer: for this we monitored by kinetic null ellipsometry the correlated time variation of the monolayer thickness. Given the problems in obtaining a good signal to noise ratio in these measurements, it was difficult to obtain precisely the functional form of the time relaxation. For simplicity we have used a single exponential form, from which we obtained a rough measure of the relaxation time τ. We have then tried to determine the dependence of τ on temperature. However, we had upper and lower limits to the possible temperature variation with our apparatus in its present form, so again only qualitative indications could be drawn from our main results, namely, that there is an indication of the existence of a glass transition at about 16 °C for the Langmuir monolayer. Clearly such an investigation needs be made more quantitative both by extending the temperature range and improving the statistics before any definitive conclusions can be drawn.

V. CONCLUSIONS

In this paper, we reported a detailed study of photoinduced changes in the microscopic structure of monolayers, multilayers, and superlattices of a fragile polymeric liquid crystalline glass. First, we have quantitatively confirmed the interpretation given to the thickness dependence of the glass transition phenomenology we had observed.

In particular we have shown that the layered structure, which should be expected from the LS deposition technique, is conserved only up to the first four to six monolayers; for the following monolayers the structure is no more layered, leading to a homogeneous glassy structure, nevertheless the sample thickness remains linearly proportional to the number of deposited layers.

Furthermore, the similarity of the structures obtained by x-ray reflectometry and GID for the different confinement geometries of the polymer indicate that the structural and morphological photoinduced changes are connected to the relaxation of the mesogenic side chains, with the main chain providing a template structure. This indicates the predominance of side chain interactions over the effects of the free surface, or the interactions with the substrate. Thus this system could be quite useful to study intrinsic dynamical effects

of geometrical confinement, in particular for the fundamental understanding of the glass transition.

A first qualitative confirmation of this is provided by our data on the Langmuir monolayer, which suggest that the temperature dependence of the monolayer back-relaxation times indicates the presence of a glass transition, at a slightly lower temperature than for the bulk. This result, although needing more quantitative confirmation, could provide the simplest case of the truly two dimensional glass, or at least of a disordered system in which the relative weight of in-plane and out-of-plane interactions can be varied.

Another consequence of our study is the possibility of generating nanoglasses with controlled size and morphology by using the optically induced dewetting of the LS multilayers. We are currently investigating this aspect of our system, especially the effects of optical pumping, temperature and aging time on the size distribution of the polymeric glassy nanoparticles.

Finally, the effects of confinement also show up in the different response to the optical pumping shown by the multilayers relatively to the superlattices. The very same polymeric multilayer, when confined between the Ba-behenate bilayers, expands but little under the action of the pumping light: essentially, only the last layer expands. In the free multilayer instead, the expansion is proportional to the overall thickness. This difference indicates an important role of the periodic superlattice structure, which acts like a rigid cage in which the polymer is confined. Work is in progress to explore the effect of other confining media.

[1] *Side Chain Liquid Crystal Polymers*, edited by C. B. Mc Ardle (Blackie and Sons, Glasgow, 1989); *Polymeric Liquid Crystals*, edited by A. Blumstein (Plenum Press, New York, 1985); *Liquid-Crystal Polymers*, edited by N. A. Plate (Plenum Press, New York, 1993).

[2] S. Kumar, Chem. Rev. **89**, 1915 (1989); K. Anderle, R. Birenheide, M. J. A. Werner, and J. H. Wendorff, Liq. Cryst. **9**, 691 (1991).

[3] S. Hvilsted, F. Andruzzi, C. Kulima, H. W. Siesler, and P. S. Ramanujan, Macromolecules **28**, 2172 (1995); M. P. Fontana, C. Paris, and M. Polli, Mol. Cryst. Liq. Cryst. Sci. Technol., Sect. A **304**, 207 (1997).

[4] L. Cristofolini, P. Facci, P. Camorani, and M. P. Fontana, J. Phys.: Condens. Matter **11**, A359 (1999).

[5] L. Cristofolini, S. Arisi, and M. P. Fontana, Synth. Met. **124**, 151 (2001).

[6] L. Cristofolini, M. P. Fontana, M. Laus, and B. Frick, Phys. Rev. E **64**, 061803 (2001).

[7] L. Andreozzi, M. P. Fontana, F. Francia, M. Giordano, D. Leporini, and M. Rateo, J. Non-Cryst. Solids **172**, 943 (1994).

[8] *Langmuir-Blodgett Films*, edited by G. Roberts (Plenum Press, New York, 1990); *Ultrathin Organic Films*, edited by A. Ulman (Academic Press, Boston, 1991).

[9] L. Cristofolini, M. P. Fontana, and O. Konovalov, Philos. Mag. B **82**, 523 (2002).

[10] *Liquids, Freezing and Glass Transition*, edited by J. P. Hansen, D. Levesque, and J. Zinn-Justin (North-Holland, Amsterdam, 1991); W. Gotze, J. Phys.: Condens. Matter **11**, A1 (1999).

[11] E. Jenckel, Z. Phys. Chem., Stoechiom. Verwandtschaftsl. **184**, 309 (1939).

[12] G. Adam and J. H. Gibbs, J. Phys. Chem. **43**, 139 (1965).

[13] E. Donth, J. Non-Cryst. Solids **131**, 204 (1991).

[14] For a review see, e.g., K. L. Ngai, J. Phys.: Condens. Matter **11**, A119 (1999), and Refs. [18–35] therein.

[15] J. L. Keddie, R. A. L. Jones, and R. A. Cory, Europhys. Lett. **27**, 59 (1994).

[16] J. A. Forrest, K. Dalnoki-Veress, J. R. Stevens, and J. R. Dutcher, Phys. Rev. Lett. **77**, 2002 (1996).

[17] J. H. van Zanten, W. E. Wallace, and W. Wu, Phys. Rev. E **53**, 2053 (1996).

[18] B. Jerome and J. Commandeur, Nature (London) **386**, 589 (1997).

[19] L. Cristofolini, S. Arisi, and M. P. Fontana, Phys. Rev. Lett. **85**, 4912 (2000).

[20] G. B. DeMaggio, W. E. Frieze, D. W. Gidley, Ming Zhu, H. A. Hristov, and A. F. Yee, Phys. Rev. Lett. **78**, 1524 (1997).

[21] K. Fukao and Y. Miyamoto, Phys. Rev. E **61**, 1743 (2000).

[22] A. S. Angeloni, D. Caretti, C. Carlini, E. Chiellini, G. Galli, A. Altomare, A. Solaro, and M. Laus, Liq. Cryst. **4**, 513 (1989).

[23] Yu. M. Lvov, O. B. Gurskaya, T. S. Berzina, and V. I. Troitsky, Thin Solid Films **182**, 283 (1989); Yu. M. Lvov, V. I. Troitsky, and L. A. Feigin, Mol. Cryst. Liq. Cryst. **172**, 89 (1989).

[24] L. Cristofolini, T. Berzina, M. P. Fontana, and O. Konovalov, Mol. Cryst. Liq. Cryst. Sci. Technol., Sect. A **375**, 689 (2002).

[25] L. G. Parrat, Phys. Rev. **B95**, 359 (1954).

[26] L. Nevot and P. Croce, Rev. Phys. Appl. **15**, 761 (1980).

[27] C. Braun, *Parrat32 Software for Reflectivity* (HMI, Berlin, 1999).

[28] O. V. Konovalov, L. A. Feigin, and B. M. Shchedrin, Kristallografiya **41**, 640 (1996); O. V. Konovalov, I. I. Samoilenko, L. A. Feigin, and B. M. Shchedrin, *ibid.* **41**, 635 (1996).

[29] M. Stamm, G. Reiter, and K. Kunz, Physica B **173**, 35 (1991).

[30] S. Arisi, P. Camorani, L. Cristofolini, M. P. Fontana, and M. Laus, Mol. Cryst. Liq. Cryst. Sci. Technol., Sect. A **372**, 241 (2001).

[31] R. A. L. Jones and R. W. Richards, *Polymers at Surfaces and Interfaces* (Cambridge University Press, Cambridge, 1999), pp. 324–325.

[32] P. G. De Gennes, *Scaling Concepts in Polymer Physics* (Cornell University Press, Ithaca, NY, 1978).

[33] M. Daoud and G. Jannink, J. Phys. (France) **37**, 973 (1976).

[34] R. Vilanove and F. Rondelez, Phys. Rev. Lett. **45**, 1502 (1980).

[35] This holds of course only for films thin enough to avoid self-screening due to the strong absorption of the UV light by the azodye itself.